

EXPRESS LETTER

A RECENTLY DISCOVERED TRACHYTE-HOSTED RARE EARTH ELEMENT-NIOBIUM-ZIRCONIUM OCCURRENCE IN NORTHERN MAINE, USA

Chunzeng Wang,¹ John F. Slack,^{2,3,†} Anjana K. Shah,⁴ Martin G. Yates,⁵ David R. Lentz,⁶ Amber T.H. Whittaker,⁷ and Robert G. Marvinney^{7,*}

¹College of Arts and Sciences, University of Maine at Presque Isle, Presque Isle, Maine 04769

²U.S. Geological Survey (Emeritus), National Center, MS 954, Reston, Virginia 20192

³Department of Earth Sciences, Memorial University of Newfoundland, St. John's, Newfoundland A1B3X5, Canada

⁴U.S. Geological Survey, Denver Federal Center, MS 973, P.O. Box 25046, Denver, Colorado 80225

⁵School of Earth and Climate Sciences, University of Maine, Orono, Maine 04469

⁶Department of Earth Sciences, University of New Brunswick, Fredericton, New Brunswick E3B 5A3, Canada

⁷Maine Geological Survey, 93 State House Station, Augusta, Maine 04333

Abstract

Reported here are geological, geophysical, mineralogical, and geochemical data on a previously unknown trachyte-hosted rare earth element (REE)-Nb-Zr occurrence at Pennington Mountain in northern Maine, USA. This occurrence was newly discovered by a regional multiparameter, airborne radiometric survey that revealed anomalously high equivalent Th (eTh) and U (eU), confirmed by a detailed ground radiometric survey and by portable X-Ray fluorescence (pXRF) and whole-rock analyses of representative rock samples. The mineralized area occurs within an elongate trachyte body (~1.2 km²) that intrudes Ordovician volcanic rocks. Geologic constraints suggest that the trachyte is also Ordovician in age. The eastern lobe (~900 × ~400 m) of the trachyte is pervasively brecciated with a matrix containing seams, lenses, and veinlets composed mainly of potassium feldspar, albite, and fine-grained zircon and monazite. Barite is locally abundant. Minor minerals within the matrix include columbite, bastnäsite, euxenite, chlorite, pyrite, sphalerite, and magnetite. The pXRF analyses of 22 samples (App. Table A1) collected from the eastern lobe demonstrate that this entire part of the trachyte is highly mineralized. Whole-rock geochemical analyses for samples from the eastern lobe document high average contents of Zr (1.17 wt %), Nb (1,656 ppm), Ba (3,132 ppm), Y (1,140 ppm), Hf (324 ppm), Ta (122 ppm), Th (124 ppm), U (36.5 ppm), Zn (689 ppm), and Sn (106 ppm). Among light REE, the highest average concentrations are shown by La (763 ppm) and Ce (1,479 ppm). For heavy REE (HREE), Dy and Er are the most abundant on average (167 and 114 ppm, respectively). No HREE-rich minerals such as xenotime have been identified; the HREE may reside chiefly in monazite and bastnäsite, and within the fine-grained zircon. Very strong positive correlations (R²) of 0.92 to 0.98 exist between Th and Zr, Nb, Y, Ce, Yb, and Sn, indicating that the radiometric data for eTh are valid proxies for concentrations of these metals in the mineralized rocks.

Trachyte-hosted REE-Nb-Zr deposits like the occurrence at Pennington Mountain also are known in eastern Australia and in the south Qinling belt of Central China. Based on comparisons with these deposits, and the lack of detailed geologic mapping in the Pennington Mountain region, we suggest that other rare-metal occurrences contained in trachyte may exist elsewhere in northern Maine, and more widely in the Appalachian-Caledonian orogen where volcanic and subvolcanic trachytes have been recognized.

Introduction

Critical minerals are increasingly important for diverse types of industries and a low-carbon energy future. In the United States, the U.S. Geological Survey in 2022 designated 50 mineral commodities as being critical, i.e., essential to the economy and security of the nation, but for which there is risk of supply chain disruption (Nassar and Fortier, 2021; U.S. Geological Survey, 2022a). Included in this list are rare earth elements (REE), niobium, and zirconium. In 2021, the United States was 100% reliant on imports of niobium and 90% reli-

ant on imports of REE; in previous years the United States had been 100% reliant on imports for both (U.S. Geological Survey, 2022b). Except for the Mountain Pass REE mine in southern California, no current production from U.S. deposits exists for REE or for niobium. In this report, we present preliminary field and laboratory data on a recently discovered trachyte-hosted REE-Nb-Zr occurrence in northern Maine and compare it with similar deposits in Australia and China.

Discovery

The U.S. Geological Survey Earth Mapping Resources Initiative (Earth MRI), a national mapping and data collection effort by the U.S. Geological Survey and state geological sur-

[†]Corresponding author: e-mail, jfslack@usgs.gov

*Present address: P.O. Box 615, Readfield, Maine 04355.

veys, was developed to improve knowledge of the nation's geology and document areas that may have potential for critical mineral resources (Day, 2019; U.S. Geological Survey, 2022c). This initiative includes the collection of airborne geophysical data. In the summer of 2021, an airborne magnetic and radiometric survey was contracted and flown in northern Maine over the Munsungun-Winterville belt and vicinity, covering an area of ca. 9,600 km² (Shah, 2022; Fig. 1). This region was selected because of the presence of the large, 30-Mt Ordovician Bald Mountain Cu-Zn-Ag-Au(-Co-Sb-Se-Te-Bi) volcanogenic massive sulfide (VMS) deposit (Slack et al., 2003) and large stratiform Mn deposits hosted in Silurian sedimentary rocks northeast of the volcanic terrane (total 327 Mt @ 9.0 wt % Mn; Pavlides, 1962; Slack et al., 2022), and the potential for additional VMS and other deposit types that might contain critical metals. The new airborne radiometric data (gamma-ray spectrometry for K, eU, and eTh) generally show low values of eTh except for an anomaly on the eastern side of Pennington Mountain (Fig. 2A) that resides within a slightly larger region having elevated K. The area associated with these anomalies

subsequently has been characterized geologically via mapping and sampling, and by a ground-based radiometric survey.

Geophysical Data

The airborne geophysical data were collected with the goal of imaging the geologic framework of the VMS and sediment-hosted Mn deposits known to be present in the region. The data were collected along NW-flight lines, oblique to the northeast structural trends of the region, with a line spacing of 250 m and nominal flying height of 80 m above ground; areas with rugged topography were flown at greater heights for safety reasons. The airborne radiometric data, which represent sources within the upper 0.5 to 1 m (excluding vegetation), have a horizontal resolution of several hundred meters. Downloadable data and details of the processing are provided in Shah (2022).

Over most of the survey area, the airborne data show that radiometric thorium (commonly referred to as equivalent thorium or eTh because of multiple decay chains involved in the estimate) is typically subdued with eTh <10 ppm. These

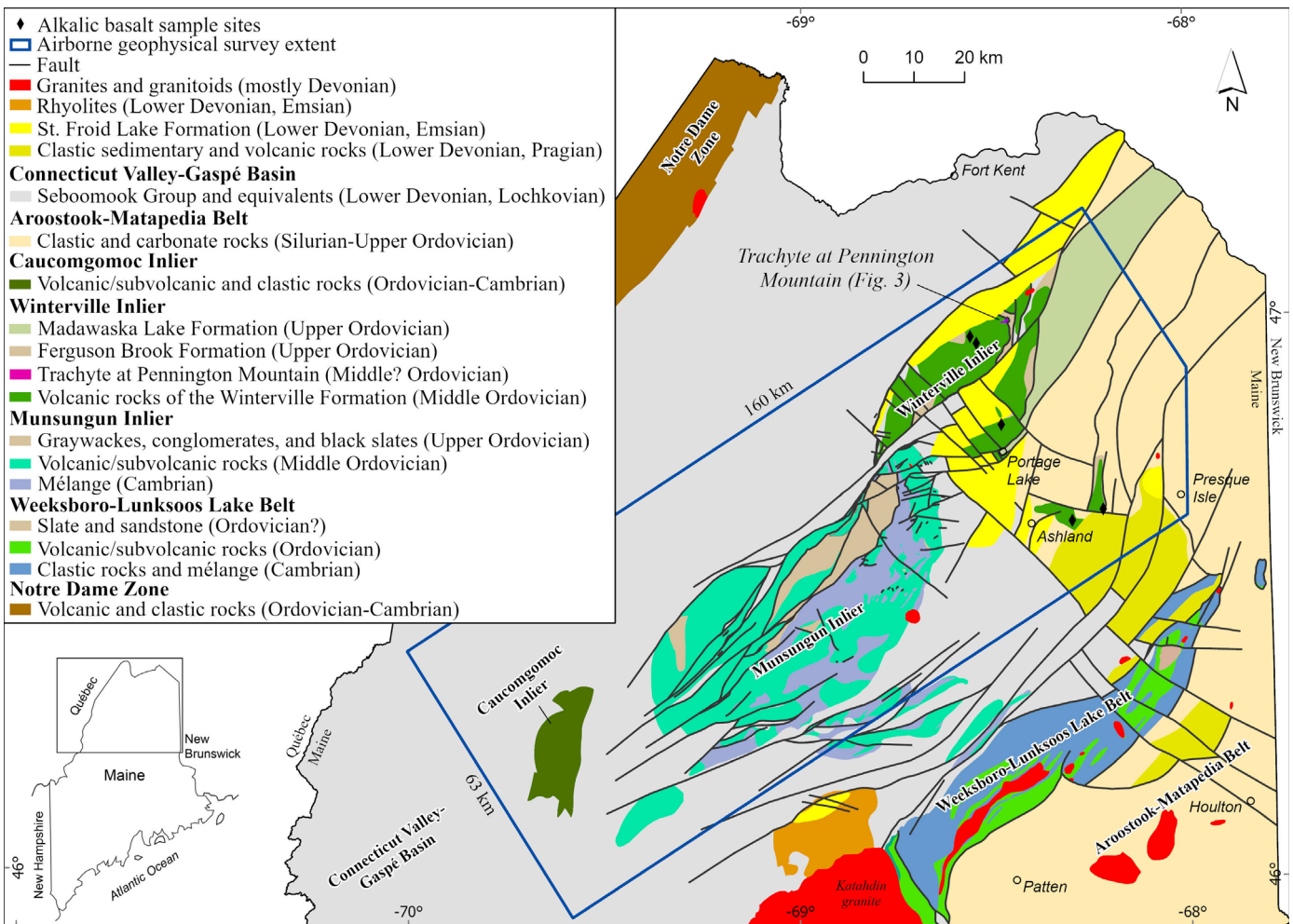


Fig. 1. Simplified regional geologic map of northern Maine showing location of Pennington Mountain trachyte-hosted REE-Nb-Zr occurrence within the area covered by regional U.S. Geological Survey airborne radiometric and magnetic survey in northern Maine (inset shows location). Geology is based on recent detailed mapping (Wang, 2018, 2019, 2021a, b, 2022a, b; Pollock, 2020) and unpublished reconnaissance mapping by C. Wang. St. Froid Lake and Ferguson Brook formations are after Wang (2022a). Diamond symbols are locations of alkalic basalts reported by Winchester and van Staal (1994).

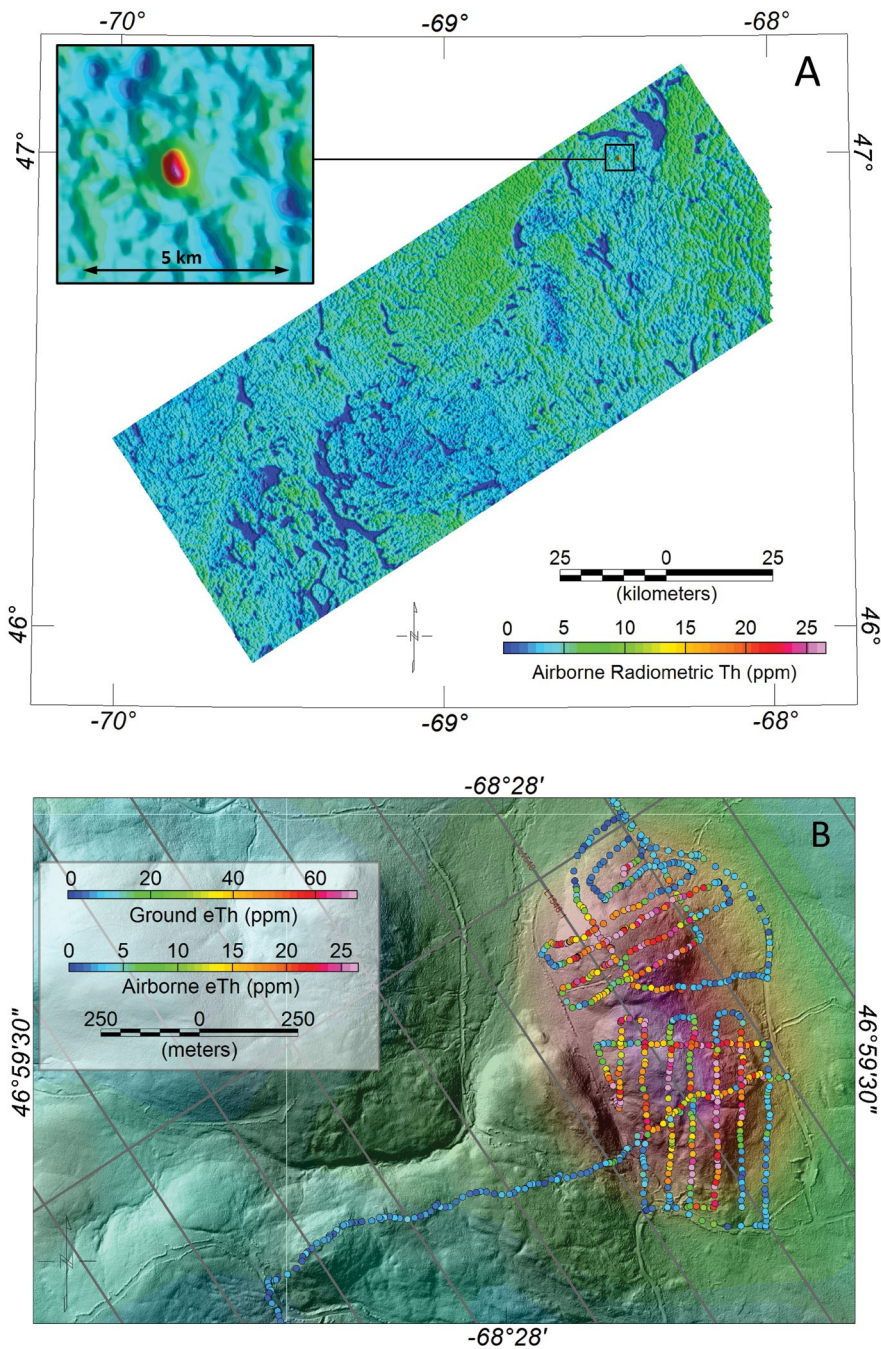


Fig. 2. A. Radiometric thorium from the airborne survey. Inset shows detail of Pennington anomaly. Dark blue areas (lowest values) in regional survey area represent lakes. B. Radiometric eTh draped over a lidar-shaded relief map. Circles represent ground radiometric eTh measurements. Gray lines show flight lines of airborne survey.

generally low values are due to glacial cover throughout the area and to low amounts of Th-bearing minerals in both the igneous and sedimentary rocks; lowest values are observed over lakes as gamma rays cannot escape the fluid medium. However, in the northeastern corner of the survey area and on the eastern side of Pennington Mountain is a single anomaly with eTh values up to 26 ppm. This area with elevated eTh is approximately 900 m long by 400 m wide.

The airborne Th anomaly is crossed by only three flight lines, so a detailed ground radiometric survey was subsequently conducted to better delineate the horizontal extent of rock with elevated Th (Shah and Wang, 2022). Continuous gamma-ray spectrometer measurements were recorded by walking over

the anomaly area in a survey pattern with several cross traverses; average values were logged every 30 s. The results (Fig. 2B) show that Th-bearing minerals are widespread over the eastern part of the mountain and decrease in concentration over lower elevations associated with glacial sediments, both at the edge of the mountain and locally within stream valleys.

Geology

The Pennington Mountain radiometric eTh anomaly is confined to a trachyte body, here informally named the trachyte at Pennington Mountain (Fig. 3). The trachyte occurs in the northeast-trending Winterville inlier, which forms part of the Ordovician Munsungun-Winterville belt, both of which are in

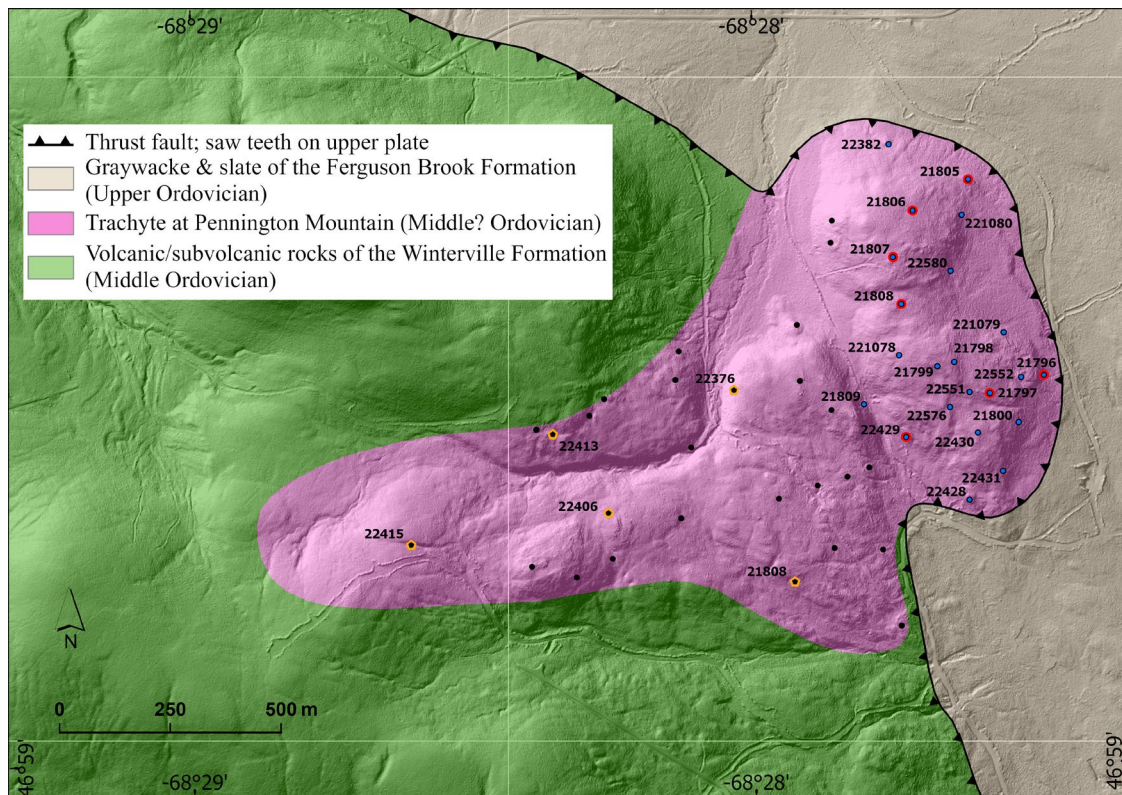


Fig. 3. Geologic map of Pennington Mountain area showing field observation sites and sample locations. Ferguson Brook Formation is after Wang (2022a). Dots of any shape and color represent field observation sites. Sites sampled for portable XRF analysis (blue circles) and whole-rock geochemical analysis (red circles for strongly mineralized eastern lobe and orange diamonds for weakly mineralized western lobe) are labeled with IDs for reference to Tables A1 and A2.

a region of northern Maine characterized by sub-greenschist (prehnite-pumpellyite) grade metamorphism. The inlier is underlain predominantly by volcanic rocks of the Middle Ordovician Winterville Formation (Boone, 1958) with lesser Upper Ordovician graywacke and black slate of the Ferguson Brook Formation of Wang (2022a), all unconformably overlain by pre-Acadian sedimentary rocks of the Lower Devonian Sebomook Group and clastic sedimentary rocks of the post-Acadian St. Froid Lake Formation of Wang (2022a) (Fig. 1). The rocks have been significantly displaced by Acadian and post-Acadian faulting dominated by southeast-directed thrust faults of at least two generations. The Winterville Formation is chiefly basalt with lesser pyroclastic rocks (tuff, lapillistone, and breccia), diabase, rhyolite, dacite, and trachyte. The extrusive flows and pyroclastic rocks are tilted due to Acadian and post-Acadian folding and faulting, and strike mainly northeast-southwest. The basalt is mostly aphyric, typically showing pillows and vesicles/amygdules and, less commonly, peperite and hyaloclastite textures. Whole-rock geochemical analyses of eight basalt samples collected from the Fish River Lake-Pennington Mountain area (Wang, 2022a, b) demonstrate that the basalt is largely transitional between calc-alkaline and tholeiitic, depleted in Ta and Nb, moderately enriched in light REE (LREE), and has normalized trace element patterns and tectonic discrimination signatures that suggest formation in an ensialic volcanic arc. These results are similar to the conclusions of previous geochemical studies of the Winterville Formation by Hynes (1976) and Winchester and van Staal

(1994). The trachyte at Pennington Mountain, approximately ~1.2 km² in area, forms an irregular, shallow intrusive body within northeast-striking basalt and minor tuff, rhyolite, and diabase sills or dikes of the Winterville Formation. The western lobe of the intrusion cuts Winterville volcanic rocks. The eastern lobe is bounded by a low-angle thrust fault against Upper Ordovician graywacke and black slate of the Ferguson Brook Formation (Fig. 3). The trachyte is massive, fine grained with a microporphyritic texture, and featureless in the field except for three outcrops in the western lobe that have vesicular and amygdaloidal textures. The elongated vesicles and quartz amygdules plunge to the west at about 15°, probably due to thrust faulting during the Early Devonian Acadian orogeny.

Sampling and Analytical Methods

Gamma-Ray Spectrometry (GRS) using a handheld GF Instruments Gamma Surveyor instrument was used to help in mapping the area and for selecting samples for further analysis. Ten samples of trachyte were collected for thin sections and polished thin sections for petrographic, micro-X-ray fluorescence (μ XRF), microprobe energy-dispersive spectrometry (EDS), and wavelength-dispersive spectrometry (WDS) analyses and imaging. Twenty-two samples evenly collected from the eastern lobe were analyzed for major and selected trace elements by portable X-ray fluorescence (pXRF) spectrometry. Twelve trachyte samples were selected for whole-rock major, trace, and REE analyses. Figure 3 shows outcrop observation stations and sampling sites within the trachyte.

Whole-rock analyses for major, trace, and REE were performed at ALS Laboratories by inductively coupled plasma-mass spectrometry after a Li borate fusion and acid digestion. Selected trace elements (As, Co, Ni, Cu, Zn, Cd, Pb, Mo, Ag, Tl) were analyzed separately by inductively coupled plasma-atomic emission spectrometry following a four-acid digestion. Details of the analytical procedures including standards are available at www.alsglobal.com. pXRF analyses (Lemière, 2018) were done at the University of New Brunswick (UNB) using an Olympus Vanta pXRF to screen samples for further analysis. A silica blank and four certified reference materials, OREAS620, OREAS146, NIST2710a, and NIST2711a, were used for calibration checks. Both the rare element geochemical mode [2 energy levels, 15 kV (120 s), 50 kV (120 s)] and soil mode [3 energy levels 10 kV (60 s), 25 kV (60 s), and 50 kV (60 s)] were used. We selected the best data analysis mode with the best R^2 value (extrapolated through the origin) for reporting the data. μ XRF-EDS elemental scans of polished thin sections of selected samples were used to document textures and guide more detailed microbeam mineralogical studies. Data were obtained at UNB using a Bruker Nano M4 Tornado μ XRF instrument, following the methods outlined in Flude et al. (2017). Operating conditions were 40 kV and 40 nA with a step size of 25 μ m for 3 ms, which generated 20- μ m square spots used to produce the scans.

Mineral identifications were done on polished thin sections at the University of Maine in Orono via EDS and WDS using a Cameca SX-100 electron microprobe with PeakSight software and a Roentec XFlash EDS detector (4036-channel resolution; EdWin software). Operating conditions for backscattered electron (BSE) imaging done via EDS were 15 kV, 20 nA, a focused beam, and 15.3- μ s dwell time, yielding images of 1,024 \times 768 pixels; WDS imaging conditions, used for identification of C and F, and for thin-section scans of K, Y, and Yb, were 15 kV, 200 nA, a focused beam, 5-ms dwell time, and a 15- μ m step size in the production of six tiled 821 \times 838-pixel images.

Textures and Mineralogy

Paragenesis and mineralogy

The trachyte is homogeneously massive and fine grained with a microporphyritic texture (Fig. 4). Euhedral perthite phenocrysts are set in a microcrystalline groundmass composed predominantly of potassium feldspar and subordinate albite, together with minor ferromagnesian silicates (likely hornblende and biotite altered to chlorite). The eastern lobe is more strongly mineralized and altered than the western lobe, and is characterized by pervasive fractures and breccia textures (Fig. 5). The REE-Nb-Zr minerals occur mostly in a texturally diverse matrix to the breccia fragments but are difficult to recognize in outcrops and hand specimens, except locally as aggregates or veins containing very small (<0.5 mm) white or pale brown grains. The μ XRF-EDS scans of entire thin sections obtained from strongly mineralized trachyte samples show distinctive breccia textures (Fig. 6) caused by intensive fracturing and element enrichments for K, Zr, Nb, La + Ce, and Zn. Results for K indicate that the highest concentrations occur in angular 0.1- to 1.0-cm fragments, with lower levels present in the surrounding matrix (Fig. 6A). High contents

of Zr, Nb, La + Ce, and Zn are largely confined to the matrix, with the fragments having only minor enrichments of these metals in veinlets and disseminations (e.g., Fig. 6B-F).

The REE-Nb-Zr minerals occur dominantly in the matrix of the breccia as seams, lenses, and veins, and as disseminations. Within our samples imaged by μ XRF, the brecciated fragments each range in size from 0.1 to at least 1 cm. Based on textures shown in the μ XRF-EDS maps (Fig. 6A) and BSE images (Fig. 7A, B), the following generalized paragenesis is proposed: (1) significant brecciation of igneous trachyte, particularly within the eastern lobe; (2) pervasive alkali metasomatism of fragments by potassium feldspar \pm albite coupled with hydrothermal mineralization of the matrix by REE-Nb-Zr phases + potassium feldspar + albite \pm magnetite \pm sphalerite \pm pyrite; and (3) filling of younger crosscutting fractures by albite, bastnäsite [(LREE)CO₃F], or barite. In some samples, relict potassium feldspar phenocrysts are partly replaced by albite (Fig. 7C). Principal secondary minerals in the breccias are jarosite, hematite, and one or more unidentified K-Al-Si clays.

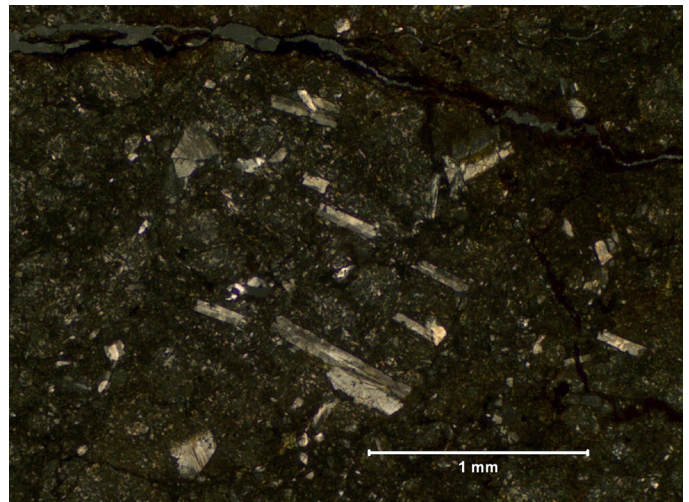


Fig. 4. Photomicrograph of trachyte (sample 21809) from Pennington Mountain showing typical microporphyritic texture. Cross-polarized light.



Fig. 5. Field photograph of strongly mineralized trachyte (sample 21807) from Pennington Mountain. Note on broken (unweathered) surface small white and brown veins that contain REE, Nb, and Zr minerals.

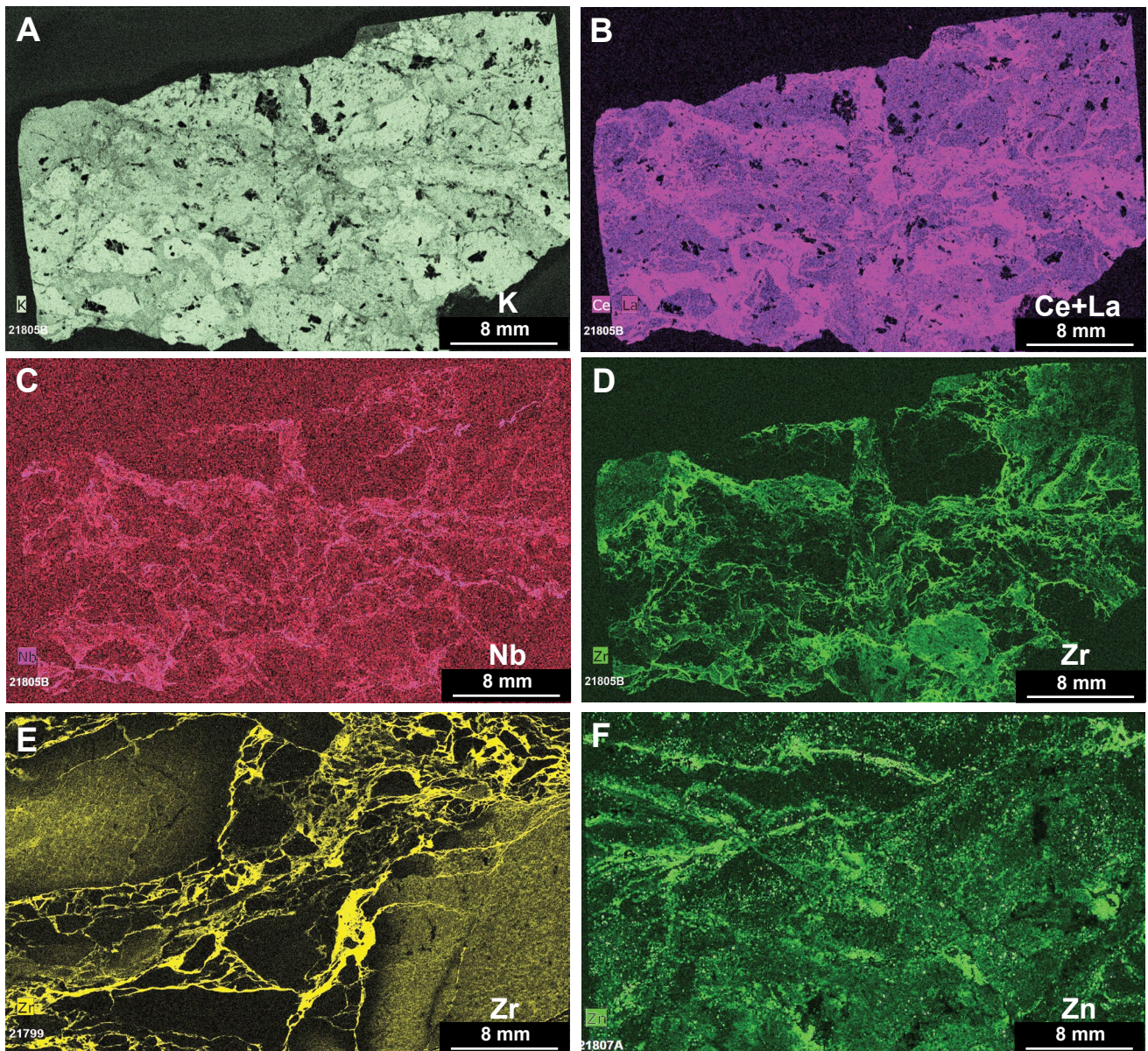


Fig. 6. μ XRF images of selected elements in mineralized trachyte from Pennington Mountain. (A) K. (B) Ce + La. (C) Nb. (D) Zr. (A-D, sample 21805B). (E) Zr, sample 21799. (F) Zn, sample 21807A. Note that in A, K is concentrated pervasively in angular fragments and less in the matrix. Most K-rich fragments lack high Zr, Nb, or LREE, or have only small veinlets containing these elements, with the highest concentrations occurring in the matrix.

Hydrothermal minerals in the matrix are dominated by potassium feldspar that contains minor to major amounts of Ba (several wt %; cores are enriched relative to rims). Other abundant hydrothermal minerals are zircon and monazite [(LREE,Th)PO₄]. The zircon typically forms bands of granular to spongy concentrations of very small (<1 μ m) grains (Fig. 7D-G); we use the term zircon here in a preliminary sense, since complete quantitative analysis for this mineral is not yet available. Uncommon, somewhat coarser zircon that forms aggregates of anhedral grains 5 to 20 μ m in diameter also occurs in the matrix (Fig. 7E). Monazite typically forms 1- to 3- μ m grains disseminated in zircon bands (Fig. 7H), or less commonly within potassium feldspar (Fig. 7D), and varies in composition from relatively low Th + U to

high Th + U (Th > U). Minor hydrothermal minerals, present in some but not all samples, are (1) bastnäsite occurring as 1- to 20- μ m grains in zircon and albite, as 1- to 3- μ m grains in pyrite, and in crosscutting veinlets (Fig. 7C); (2) euxenite [(Y,Ca,Ce,U,Th)(Nb,Ta,Ti)₂O₆] as disseminated 5- to 10- μ m grains (Fig. 7B); (3) Fe-Mg chlorite as disseminations or small irregular masses; (4) barite in euhedral disseminated grains (Fig. 7E) and veinlets; (5) columbite [FeNbO₆] as irregular grains up to 100 μ m in diameter commonly peripheral to zircon bands (Fig. 7F); (6) pyrite as disseminated 50- to 150- μ m grains associated with zircon; (7) sphalerite as subhedral to euhedral grains 1 to 50 μ m in diameter intergrown with or contained in zircon (Fig. 7G), and in aggregates of 10- to 100- μ m grains within albite and potassium feldspar;

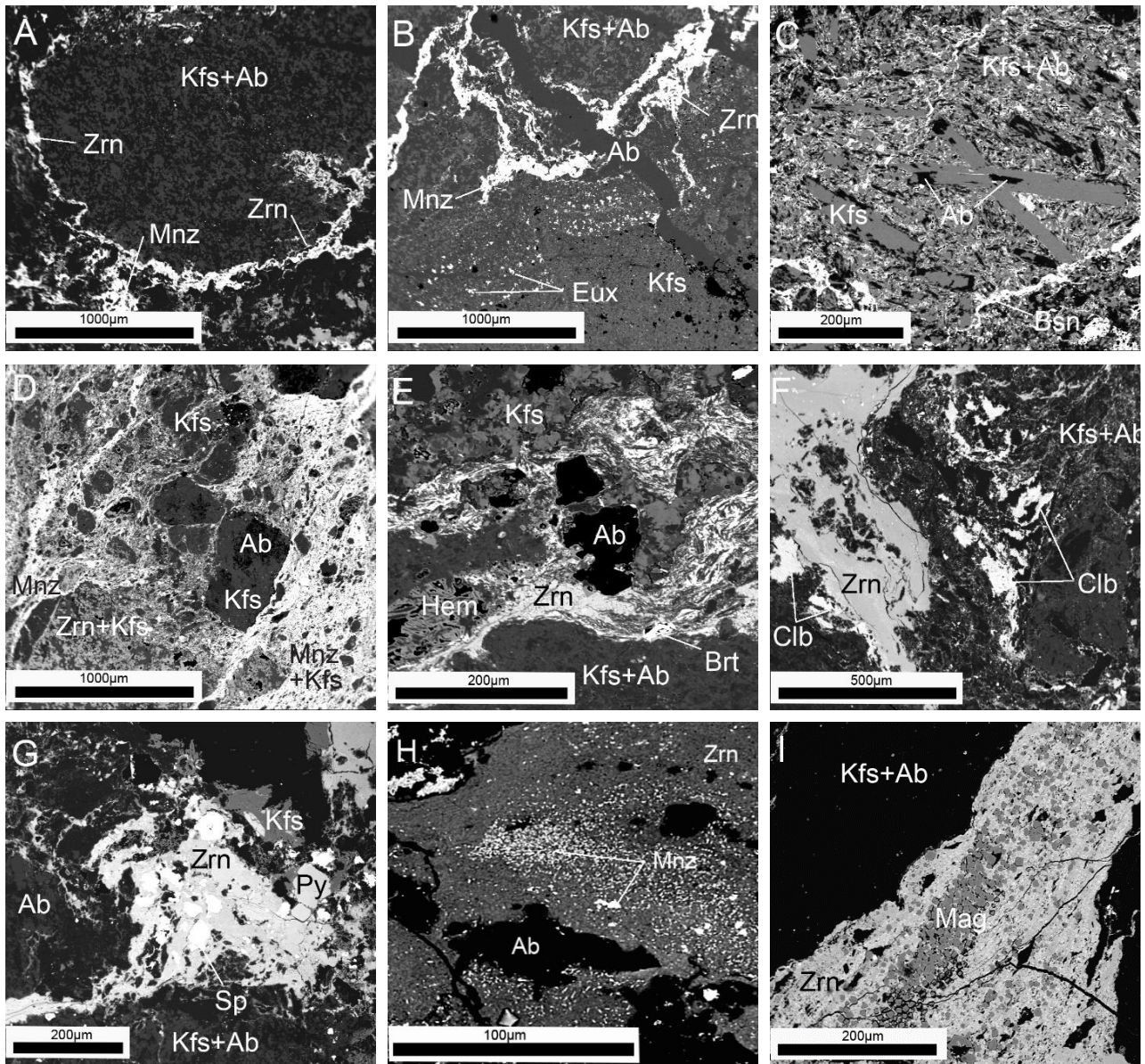


Fig. 7. Backscattered electron images showing representative textures and REE, Nb, Zr, Ba, and Zn minerals in brecciated and altered trachyte from Pennington Mountain. (A) Subrounded clast of K-feldspar and albite surrounded by matrix of zircon and minor monazite; sample 21797. (B) Albite vein cutting seams of fine-grained zircon and monazite, and blocky area with disseminated euxenite, in matrix of K-feldspar and albite; sample 21797. (C) Euhedral K-feldspar phenocrysts partly replaced by albite in matrix of K-feldspar, albite, and bastnäsite, and late bastnäsite veinlet; sample 21807. (D) Irregular seams, lenses, and veinlets of fine-grained zircon and monazite cutting K-feldspar and albite; sample 21799. (E) Seams of fine- and coarse-grained zircon with barite around albite and K-feldspar, with secondary hematite; note coarse-grained zircon in lower center of image; sample 21805. (F) Zircon and columbite in matrix of K-feldspar and albite; sample 21807. (G) Zircon with sphalerite inclusions intergrown with albite, K-feldspar, and pyrite; sample 21807. (H) Fine-grained monazite disseminated in K-feldspar, sample 21807A. (I) Euhedral magnetite in zircon; sample 21799. Abbreviations: Ab = albite, Brt = barite, Bsn = bastnäsite, Clb = columbite, Eux = euxenite, Hem = hematite, Kfs = K-feldspar, Mnz = monazite, Py = pyrite, Sp = sphalerite, Zrn = zircon.

and (8) euhedral magnetite as disseminations and aggregates in zircon (Fig. 7I). Sparse to rare hydrothermal minerals, which are typically fine-grained (<10 µm), include betafite [(Ca,U)₂(Ti,Nb,Ta)₂O₆(OH)], ilmenorutile [(Ti,Nb,Fe)O₂], siderite, galena, and cassiterite; quartz occurs in late veinlets. Heavy REE-rich minerals such as xenotime were not found. Importantly, numerous EDS spectra obtained on the Zr-silicate phase indicate that this mineral contains small

amounts of P and HREE, consistent with the results of detailed microbeam studies of zircon from other settings that show these elements can occur as crystallographic substitutions (e.g., Hoskin and Schaltegger, 2003). Noteworthy in this context is the HREE-rich hydrothermal zircon occurring in some peralkaline granites of Scotland that contains up to 0.99 wt % Dy₂O₃ and 1.27 wt % Yb₂O₃ (Belkin and Macdonald, 2021).

Geochemistry

pXRF analyses

The 22 pXRF analyses (App. Table A1) represent averages of three spots per sample. These results confirm the notably anomalous U and Th contents of all samples identified by GRS and show highly anomalous Zr (up to 2.0 wt %), Y (up to 0.14 wt %), Nb (up to 0.69 wt %), La (up to 0.03 wt %), Zn (up to 0.5 wt %), Cu (up to 0.03 wt %), and Sn (up to 0.01 wt %). Although the data are considered semiquantitative, sample selection done for follow-up lithochemical analysis used these pXRF results and the GRS data for screening purposes. Sample locations are shown in Figure 3.

Whole-rock analyses

Table 1 lists basic statistics for seven strongly mineralized samples collected from the eastern lobe and for five weakly mineralized samples from the western lobe of the trachyte at Pennington Mountain. Appendix Table A2 lists complete whole-rock data for all analyzed samples. Sample locations are shown in Figure 3.

Compared to the western lobe, average values for major elements in the strongly mineralized samples (eastern lobe) are characterized by relatively low SiO₂ (59.4 ± 1.33 wt %), TiO₂ (0.16 ± 0.05 wt %), Fe₂O₃^T (3.77 ± 1.45 wt %), MnO (0.04 ± 0.02 wt %), MgO (0.33 ± 0.33 wt %), and P₂O₅ (0.14 ± 0.08 wt %). In contrast are relatively high averages determined for Na₂O (5.75 ± 1.18 wt %) and K₂O (5.91 ± 1.55 wt %). Low major-element totals mostly reflect high zirconium contents and unanalyzed sulfur and fluorine. The trace elements with the highest concentrations are Zr (11,706 ± 2,144 ppm), Nb (1,656 ± 405 ppm), Ba (3,132 ± 4,506 ppm; one sample has 1.32 wt %), and Ce (1,479 ± 410 ppm). Relatively high averages are also evident for Y (1,140 ± 305 ppm), Hf (324 ± 59.4 ppm), Zn (689 ± 616 ppm), Ta (122 ± 22.2 ppm), Th (124 ± 16.5 ppm), U (36.5 ± 12.5 ppm), and Sn (106 ± 22.0 ppm). Among LREE, in addition to Ce, the highest average concentrations observed are for La (763 ± 245 ppm) and Nd (489 ± 146 ppm); for HREE, Dy and Er are the most abundant on average (167 ± 42.7 and 114 ± 31.1 ppm, respectively). Total Y+REE oxides average 5,613 ± 1,512 ppm. Chondrite-normalized Ce anomalies are negligible (1.11 ± 0.07); Eu displays uniformly moderate negative anomalies (Eu/Eu* = 0.16 ± 0.01).

Weakly mineralized samples, from the western lobe, on average contain appreciably higher SiO₂, TiO₂, and Fe₂O₃^T, and lower Al₂O₃ (Table 1). Among trace elements of interest for this study, the weakly mineralized samples have much lower average contents of REE, Y, Zr, Nb, Hf, Ta, Ba, Th, U, Sn, and Zn than the strongly mineralized samples from the eastern lobe. Also noteworthy in two samples are slightly higher positive Ce anomalies and much smaller negative Eu anomalies relative to those from the eastern lobe of the trachyte body. Among all 12 analyzed samples, very strong positive correlations (R²) exist between Th and Zr (0.98), Nb (0.94), Y (0.95), Ce (0.92), Yb (0.95), and Sn (0.94); moderately strong correlations occur for Th vs La (0.87), Nd (0.87), and U (0.84).

Figure 8 shows a chondrite-normalized plot of REE data for strongly and weakly mineralized samples of trachyte from Pennington Mountain together with data for several major REE deposits, including the carbonatite-hosted Bayan Obo (China) and Mountain Pass (California) deposits, and the al-

kaline igneous-hosted deposits at Bokan Mountain (Alaska) and Toongi (Dubbo) (Australia). Toongi is a REE-Nb-Zr deposit also hosted by trachyte. Shown for comparison are the range and average for seven Cenozoic unmineralized trachytes, which have REE abundances ca. 10× lower than those of the strongly mineralized Pennington Mountain samples. Chondrite-normalized data for the strongly mineralized Pennington Mountain samples display relatively flat patterns in which La abundances are ~1,500× to ~4,000× and Yb abundances are ~500× to ~1,000× chondritic values. No significant Ce anomalies are evident. All samples from this eastern lobe of the trachyte body show moderately negative Eu anomalies.

Discussion

Delineation of REE-Nb-Zr mineralization at Pennington Mountain

The strongly and pervasively mineralized nature of the eastern lobe of the trachyte body is delineated on the basis of a detailed ground GRS survey (Fig. 2B), pXRF analyses of 22 evenly distributed samples (App. Table A1), and whole-rock geochemical data for seven samples (App. Table A2). Together with the eTh values obtained from the airborne radiometric survey, these data indicate that the REE-Nb-Zr mineralization is widespread in this part of the trachyte and that the analyzed samples are representative. Importantly, very strong positive correlations (R²) of 0.92 to 0.98 that exist in the whole-rock geochemical data (*n* = 12) between Th and Zr, Nb, Y, Ce, Yb, and Sn indicate that the GRS data for eTh represent valid proxies for concentrations of these metals in the trachyte.

Interpretation of REE-Nb-Zr genesis

A preliminary interpretation of the genesis of REE-Nb-Zr mineralization at Pennington Mountain is presented here on

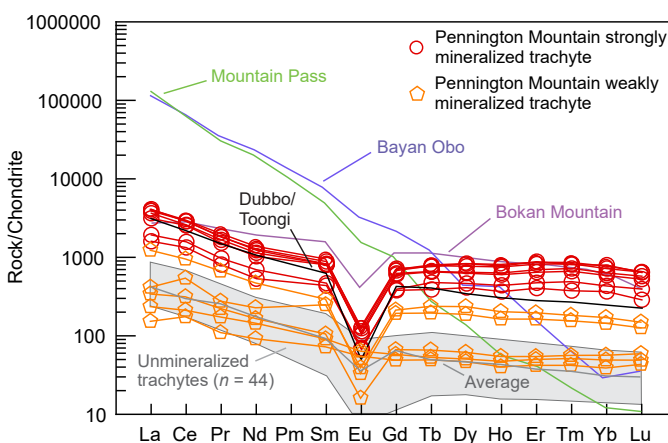


Fig. 8. Chondrite-normalized REE plot of whole-rock data for seven strongly mineralized and five weakly mineralized trachyte samples from Pennington Mountain. Included for comparison are average or typical analyses for Bayan Obo (China) REE-Nb-Fe carbonatite ore (Yang et al., 2009), Mountain Pass (California) carbonatite ore (Verplanck et al., 2016), Bokan Mountain (Alaska) REE-rich peralkaline dikes (Tetra Tech, 2013), and the Toongi (Australia) REE-Nb-Zr deposit (Spandler and Morris, 2016). Also shown are range and average REE concentrations for 42 samples from seven unmineralized Cenozoic trachytes; data from Storey (1982), Wyers and Barton (1987), Basu et al. (1991), Widom et al. (1992), White et al. (2009), Hagos et al. (2010), and Brenna et al. (2014). Chondrite values from Sun and McDonough (1989).

Table 1. Basic Statistics for Mineralized Trachyte from Pennington Mountain, Northern Maine

	Strongly mineralized (n = 7)				Weakly mineralized (n = 5)			
	Average	S.D.	Min	Max	Average	S.D.	Min	Max
SiO ₂ (wt %)	59.4	1.33	57.6	61.3	62.3	3.12	58.9	67.1
TiO ₂	0.16	0.05	0.12	0.25	0.39	0.36	0.11	0.91
Al ₂ O ₃	17.6	0.49	16.85	18.15	15.5	1.47	14.0	17.4
Fe ₂ O ₃ ^T	3.77	1.45	1.94	6.23	5.30	2.26	2.42	8.54
MnO	0.04	0.02	0.01	0.06	0.11	0.02	0.07	0.13
MgO	0.33	0.33	0.09	1.04	0.57	0.35	0.10	0.98
CaO	0.09	0.03	0.06	0.14	0.72	1.27	0.03	2.98
Na ₂ O	5.75	1.18	4.63	7.60	5.88	1.82	4.35	8.99
K ₂ O	5.91	1.55	3.69	7.73	3.21	1.94	0.10	5.19
P ₂ O ₅	0.14	0.08	0.04	0.28	0.15	0.16	0.03	0.40
BaO	0.32	0.45	0.06	1.32	0.10	0.12	0.01	0.31
LOI	3.14	1.31	2.15	6.03	4.79	1.06	3.68	6.17
Total	96.65	1.50	94.54	98.91	99.04	0.98	98.07	100.61
Li (ppm)	15.7	11.3	10	40	15	10	<10	20
Ga	143	43	84.5	194	53.4	25.1	23.9	87.7
Sc	<1	<1	<1	<1	4.0	4.2	<1	9
V	12.9	12.9	<5	41	<5	0	<5	<5
Cr	9.3	1.9	5	10	5.8	3.4	<5	11
Nb	1,656	405	1,200	2,160	262	251	59.2	605
Ta	121.8	22.2	89.2	143.5	17.6	17.1	3.70	41.2
Zr	11,706 ¹	2,144 ¹	8,410	13,862 ¹	2,331	1,764	868	4,760
Hf	324.3	59.4	233	384	59.6	50.1	17.2	128
Th	123.7	16.52	98.6	142.5	21.08	18.05	5.23	45.5
U	36.5	12.5	19.8	53.4	6.14	4.74	1.65	11.6
Sn	105.9	22.0	78.0	135	26.0	24.4	4.90	59.2
W	1.8	2.4	<0.5	7	<5	0	<5	<5
As	44.0	23.4	9.0	67.0	4.0	2.2	<5	8
Co	1.1	1.3	<0.5	4.0	1.4	0.5	1	2
Ni	0.9	0.9	<1	3	2.8	1.3	2	5
Cu	8.1	2.9	4.0	13	6.6	3.6	3	12
Zn	689.0	616.3	54.0	1720	242.6	203.5	127	603
Cd	2.0	1.5	<0.5	3.7	0.4	0.3	<0.5	0.9
Pb	124.3	30.1	81.0	167	19.8	23.3	5	61
Mo	3.4	3.9	<1	12	2.8	3.5	1	9
Ag	3.5	1.7	<0.5	5.3	<0.5	<0.5	<0.5	<0.5
Tl	<10	<10	<10	<10	<10	<10	<10	<10
Cs	1.19	0.58	0.56	2.14	0.44	0.29	0.15	0.88
Rb	174.1	28.65	132.5	200	53.92	25.31	15.00	78.60
Sr	91.1	28.5	42.2	129	64.0	51.9	18.7	149
Ba	3,132	4506	531	13,200	918	1,110	55.2	2,840
Y	1,140	305	649	1,415	154	115	63.1	299
La	762.6	245.4	383	981	111.6	101.9	35.9	289
Ce	1,479	409.5	824	1,815	266.2	194.2	106	577
Pr	145.3	43.44	77.5	189.5	27.32	20.71	10.35	62.9
Nd	489.4	146.4	252	640.0	101.9	68.7	42.4	218
Sm	114.0	31.02	67.4	144.5	24.56	15.29	10.95	44.3
Eu	5.95	1.43	3.92	7.34	2.38	1.07	0.92	3.66
Gd	120.9	29.07	78.7	149	23.58	16.28	9.97	43.3
Tb	24.3	5.88	14.7	29.6	4.45	3.30	1.83	8.78
Dy	167.2	42.69	105.5	213	29.29	22.28	11.8	59.2
Ho	35.7	9.68	20.9	45.6	5.71	4.26	2.26	11.4
Er	113.8	31.11	67.6	147	16.60	11.95	6.89	32.2
Tm	17.39	4.65	9.67	21.7	2.46	1.67	1.06	4.61
Yb	105.2	28.0	62.9	136.5	15.50	10.27	6.55	28.8
Lu	13.63	3.62	7.37	16.65	2.15	1.23	1.09	3.76
(La/Yb) _{CN}	5.18	1.04	3.7	6.97	5.14	2.30	2.43	8.53
Ce/Ce [°] _{CN}	1.11	0.07	1.04	1.20	1.25	0.23	1.06	1.59
Eu/Eu [°] _{CN}	0.16	0.01	0.15	0.16	0.46	0.40	0.14	0.92
ΣREE+Y oxides	5,613	1,512	3,382	6,887	914.6	641.2	363.5	1,877

Notes: Total iron reported as Fe₂O₃, for calculation purposes, analyses below detection limits are assigned one-half that value (Sanford et al., 1993)

Ce anomalies (Ce/Ce[°]) calculated using the formula: Ce/Ce[°]_{CN} = Ce_{CN}/((La_{CN})^{0.667}·Nd_{CN}^{0.333})

Eu anomalies (Eu/Eu[°]) calculated using the formula: Eu/Eu[°]_{CN} = Eu_{CN}/((Sm_{CN})·Gd_{CN}^{0.5})

Chondrite data from Sun and McDonough (1989)

Max = maximum, Min = minimum, S.D. = standard deviation

¹ Zr data calculated for values >10,000 ppm using Zr/Hf ratio of one sample with 8,410 ppm Zr and 233 ppm Hf

the basis of field studies, petrography, and μ XRF and BSE imaging. The first stage was an episode of major brecciation that formed angular fragments mostly 1 mm to 1 cm in diameter (locally up to \sim 20 cm in outcrops), possibly due to a near-surface explosion during emplacement of the trachyte magma. Next was pervasive alkali metasomatism (Ba-rich potassium feldspar and albite) of the fragments chiefly in the eastern lobe of the trachyte that likely contributed to elevated radiometric K in the area and elevated radiometric eTh (Fig. 2B). Contemporaneous was formation of the breccia matrix composed of (1) Ba-rich potassium feldspar and albite, (2) coeval REE, Nb, Zr, and Ba minerals, and (3) minor pyrite and sphalerite (Figs. 6 and 7). This main stage of mineralization has a metal signature (in decreasing order of average concentration; Table 1) of Zr-REE-Ba-Nb-Y-Zn-Hf-Th-Ta-Sn-U. Most of the zircon observed to date is very fine grained ($<1 \mu\text{m}$) and forms textures consistent with zircon of hydrothermal origin (e.g., Rubin et al., 1989; Corfu et al., 2003). A key unanswered question is whether the hydrothermal mineralization at Pennington Mountain is related genetically to the host trachyte or instead to a younger, unexposed intrusion of similar or different composition. Geochronological work is needed in order to establish the age of the intrusion and of the hydrothermal mineralization.

Comparison with major trachyte-hosted REE-Nb-Zr deposits

Trachyte-hosted REE-Nb-Zr deposits similar to the occurrence at Pennington Mountain have not been reported previously in the United States but are known in Australia and China. The unmined Dubbo (Toongi) deposit in New South Wales, occurring within a small (\sim 0.3 km²) Cretaceous trachyte laccolith, consists of complex Na-Ca-Fe-Zr-Y-REE silicate minerals (mainly eudialyte) together with lueshite/natroniobite and minor bastnäsité dispersed uniformly throughout the intrusion (Spandler and Morris, 2016). This deposit has a [Australasian] Joint Ore Reserves Committee (JORC)-defined proven reserve of 18.9 Mt averaging 1.85 % ZrO₂, 0.871 % Σ Y+REE oxides, 0.440 % Nb₂O₅, 0.040 % HfO₂, and 0.029 % Ta₂O₅, and a measured + inferred resource of 75.2 Mt averaging 1.89 % ZrO₂, 0.740 % Σ Y+REE oxides, 0.440 % Nb₂O₅, 0.040 % HfO₂, and 0.030 % Ta₂O₅ (ASM Ltd., 2018). By comparison, the seven strongly mineralized and altered surface samples analyzed in this study from the Pennington Mountain occurrence have lower average concentrations of these components (1.58 % ZrO₂, 0.561 % Σ Y+REE oxides, 0.237 % Nb₂O₅, 0.038 % HfO₂, and 0.015 % Ta₂O₅). Importantly, abundances of HREE and HREE/LREE ratios for samples from Pennington Mountain are higher than those of carbonate-hosted deposits and the Dubbo (Toongi) deposit, and are similar to those of the Bokan Mountain deposit (Fig. 8).

The unmined Brockman REE-Nb-Zr deposit in Western Australia is within a Paleoproterozoic rhyolitic tuff in a predominantly trachytic volcanic sequence (Taylor et al., 1995a, b). This aerially extensive deposit has a JORC indicated + inferred resource of 41.4 Mt averaging 0.90 % ZrO₂, 0.210 % Σ Y+REE oxides, and 0.359 % Nb₂O₅ (Hastings Technology Metals Ltd., 2022). Major economically important minerals are hydrous, gel-like ($<1 \mu\text{m}$) zircon (similar to Pennington Mountain) that has very high average concentrations of Y

(4.49 wt %), Nb (0.77 wt %), Th (0.70 wt %), and HREE (e.g., 0.60 wt % Yb), together with variable amounts of columbite, bastnäsité, thorite, parisite, synchysite, and sphalerite in gangue dominated by fluorite and Fe-rich carbonates (Ramsden et al., 1993; Taylor et al., 1995a).

Numerous unmined REE-Nb-Zr deposits in the south Qinling orogenic belt of Central China are hosted in trachyte intrusions of Permian and Triassic age (Jiang et al., 2020; Yin and Song, 2022). The Tudiling deposit, apparently the largest, comprises 122.5 Mt at low grades averaging 0.17 % ZrO₂, 0.08 % Nb₂O₅, 0.03 % Σ REE oxides, and 0.005 % Ta₂O₅ (Xiong et al., 2018; Yan et al., 2021). Other major deposits in this belt include Zhujiayuan, Pingli, Zhuxi, and Tianbao (Nie et al., 2020a, b, 2021; Wang et al., 2021; Yan et al., 2022). These deposits form tabular lenses and vein concentrations, in both intrusive and extrusive trachyte, consisting of fine-grained monazite, bastnäsité, aeschynite, allanite, parisite, loparite, columbite, fersmite, ilmenorutile, rutile, and zircon.

Potential for similar REE-Nb-Zr occurrences elsewhere in northern Maine

Maine has a diverse metallogeny that includes a high potential for undiscovered major critical mineral deposits of stratiform manganese in sedimentary rocks, nickel-copper(-cobalt-PGEs) in mafic and ultramafic intrusions, and lithium in granitic pegmatites (Slack et al., 2022). Prior to this discovery at Pennington Mountain, no potentially economic concentrations of REE, Nb, or Zr were known in Maine (Mariano and Mariano, 2012; Van Gosen et al., 2017, 2019).

Our preliminary evaluation of the Pennington Mountain occurrence presented here assumes that trachyte is the key host rock for containing hydrothermal REE-Nb-Zr mineralization in the region. Based on the discordant geometry of the western lobe relative to strata of the host Winterville Formation and the geometry of the eastern lobe, formation as a laccolith is suggested. The trachyte intrudes volcanic rocks of the Middle Ordovician Winterville Formation. We consider it probable that this trachyte is also Middle Ordovician, but a younger yet also pre-Acadian age cannot be ruled out; the trachyte body is cut on the east side by a thrust fault (Fig. 3), which is an Acadian structure of Early Devonian age. Importantly, alkalic basalts of possible trachytic affinity have been identified elsewhere in the Winterville Formation (Winchester and van Staal, 1994) including east of Winterville, south of Portage Lake, and in the Castle Hill inlier northeast of Ashland (Fig. 1). The Middle Ordovician Pointe Verte Formation in northern New Brunswick also contains trachytic volcanic rocks (Winchester et al., 1992). The Winterville Formation has not been mapped in detail, and as a result this unit may have additional unrecognized intrusive trachyte bodies, some of which could be highly mineralized as at Pennington Mountain. Although this area was identified by a prominent eTh anomaly found during an airborne radiometric survey (Fig. 2), such surveys only image the upper 0.5 to 1 m of the land surface and hence even small amounts of glacial or soil cover will mask possible Th anomalies. Consequently, the absence of strong eTh anomalies in other areas of the Winterville Formation (Fig. 2A) does not preclude the possibility that REE-Nb-Zr occurrences like that at Pennington Mountain exist elsewhere in northern Maine. Moreover, metallogenically similar mineralization rich

in REE (and HREE) could occur within alkaline rhyolite associated with trachyte bodies, based on the geologic setting of deposits of this type such as in the Peak Range in Queensland, Australia (Chandler and Spandler, 2020).

This study of the Pennington Mountain occurrence is constrained by a lack of information on the presence and character of potential metal enrichments at depth within the trachyte body and on the age of the REE-Nb-Zr mineralization. The radiometric eTh anomaly is likely related to Th-rich monazite, which is spatially and paragenetically linked to the REE-Nb-Zr mineralization based on data from μXRF and BSE images (Figs. 6B-D; 7A, B, D, H). No separate HREE-rich minerals have been identified among our surface samples, but based on a strong correlation in whole-rock data between HREE and Th ($R^2 = 0.96$), monazite is a potential major host for some of the HREE given the lack of other identified Th-rich minerals. However, the uniformly low LREE/HREE ratios in whole-rock analyses (Fig. 8) suggest that in addition to the HREE-bearing zircon, unrecognized xenotime or other HREE-rich minerals could also be present, with or without associated monazite and independent of radiometric anomalies. Also relevant is the heterogeneous distribution of LREE and Nb minerals, on a hand-specimen scale, in contrast to the microcrystalline zircon that appears to be the most widespread hydrothermal mineral in the occurrence other than potassium feldspar.

The metal signature of hydrothermal REE-Nb-Zr mineralization at Pennington Mountain is similar to that of many deposits hosted in alkaline granites and syenites (e.g., Dostal, 2016; Beard et al., 2023). We speculate that a mineralized intrusion with this geochemical signature may exist at depth beneath the trachyte and could have been the source for the hydrothermal fluids that formed the occurrence. Importantly, the possibility of unmapped or buried alkaline granites or syenites/trachytes occurring elsewhere in the Winterville Formation cannot be ruled out and should be evaluated to better delineate potential REE-Nb-Zr resources throughout northern Maine. Similar mineralization also could exist in other areas of the Appalachian-Caledonian orogen where volcanic and subvolcanic trachytes have been recognized.

Acknowledgments

The airborne geophysical data presented here were collected and processed by Sander Geophysics and funded by the U.S. Geological Survey Earth Mapping Resources Initiative (<https://usgs.gov/special-topics/earthmri>). Bedrock geologic mapping in northern Maine was funded through the U.S. Geological Survey STATEMAP component of the National Cooperative Geologic Mapping Program and by the Maine Geological Survey. We thank Maine State Geologist Steve Dickson for support, Steve Pollock for discussions of regional geology, David Putnam for fieldwork support, and student interns Preston Bass and Liam Daniels for field assistance. Helpful reviews and suggestions on an early version of the manuscript were provided by Brad Van Gosen, Warren Day, and Editor Larry Meinert. We also thank Iain Samson for a thorough and constructive review that significantly improved the final paper.

Any use of trade, firm, or product names is for descriptive purposes only and does not imply endorsement by the U.S. Government.

REFERENCES

- ASM Ltd., 2018, Dubbo project status: Australian Strategic Minerals Ltd., West Perth, Western Australia, <https://asm-au.com>.
- Basu, A.R., Wang, J., Huang, W., Xie, G., and Tatsumoto, M., 1991, Major element, REE, and Pb, Nd and Sr isotopic geochemistry of Cenozoic volcanic rocks of eastern China: Implications for their origin from suboceanic-type mantle reservoirs: *Earth and Planetary Science Letters*, v. 105, p. 149–169.
- Beard, C.D., Goodenough, K.M., Borst, A.M., Wall, F., Siegfried, P.R., Dedy, E.A., Pohl, C., Hutchison, W., Finch, A.A., Walter, B.F., Elliott, H.A.L., and Brauch, K., 2023, Alkaline-silicate REE-HFSE systems: *Economic Geology*, v. 118 (in press).
- Belkin, H.E., and Macdonald, R., 2021, Zirconium-bearing accessory minerals in UK Paleogene granites: Textural, compositional, and paragenetic relationships: *European Journal of Mineralogy*, v. 33, p. 537–570.
- Boone, G.M., 1958, The geology of the Fish River Lake-Deboullie area, northern Maine: Unpublished Ph.D. thesis, Yale University, 186 p.
- Brenna, M., Price, R., Cronin, S.J., Smith, I.E.M., Sohn, Y.K., Kim, G.B., and Maas, R., 2014, Final magma storage depth modulation of explosivity and trachyte-phonolite genesis at an intraplate volcano: A case study from Ulleung Island, South Korea: *Journal of Petrology*, v. 55, p. 709–747.
- Chandler, R., and Spandler, C., 2020, The igneous petrogenesis and rare metal potential of the peralkaline volcanic complex of the southern Peak Range, central Queensland, Australia: *Lithos*, v. 358–359, <https://doi.org/10.1016/j.lithos.2020.105386>.
- Corfu, F., Hanchar, J.M., Hoskin, P.W.O., and Kinny, P., 2003, Atlas of zircon textures: Reviews in Mineralogy and Geochemistry, v. 53, p. 469–500.
- Day, W.C., 2019, The Earth Mapping Resources Initiative (Earth MRI)—Mapping the nation's critical mineral resources (ver. 1.1, March 2019): U.S. Geological Survey Fact Sheet 2019–3007, 2 p., <https://doi.org/10.3133/fs20193007>.
- Dostal, J., 2016, Rare metal deposits associated with alkaline/peralkaline igneous rocks: Reviews in Economic Geology, v. 18, p. 33–54.
- Flude, S., Haschke, M., and Storey, M., 2017, Application of benchtop micro-XRF to geological materials: *Mineralogical Magazine*, v. 81, p. 923–948.
- Hagos, M., Koeberl, C., Kabeto, K., and Koller, F., 2010, Geochemical characteristics of the alkaline basalts and the phonolite-trachyte plugs of the Axum area, northern Ethiopia: *Austrian Journal of Earth Sciences*, v. 103, p. 153–170.
- Hastings Technology Metals Ltd., 2022, Brockman project: <https://hastings-techmetals.com/projects/brockman/>.
- Hoskin, P.W.O., and Schaltegger, U., 2003, The composition of zircon and igneous and metamorphic petrogenesis: Reviews in Mineralogy and Geochemistry, v. 53, p. 27–62.
- Hynes, A., 1976, Magmatic affinity of Ordovician volcanic rocks in northern Maine, and their tectonic significance: *American Journal of Science*, v. 276, p. 1208–1224.
- Jiang, S., Su, H., Xiong, Y., Liu, T., Zhu, K., and Zhang, L., 2020, Spatial-temporal distribution, geological characteristics and ore-formation controlling factors of major types of rare metal mineral deposits in China: *Acta Geologica Sinica*, v. 94, p. 1757–1773.
- Lemière, B., 2018, A review of pXRF (field portable X-ray fluorescence) applications for applied geochemistry: *Journal of Geochemical Exploration*, v. 188, p. 350–363.
- Mariano, A.N., and Mariano, Jr., A., 2012, Rare earth mining and exploration in North America: *Elements*, v. 8, p. 369–376.
- Nassar, N.T., and Fortier, S.M., 2021, Methodology and technical input for the 2021 review and revision of the U.S. Critical Minerals List: U.S. Geological Survey Open-File Report 2021–1045, 31 p., <https://doi.org/10.3133/ofr20211045>.
- Nie, X., Wang, Z., Chen, L., Yin, J., Xu, H., Fan, L., Chen, P., and Wang, G., 2020a, Mineralogical constraints on Nb-REE mineralization of the Zhujayuan Nb (-REE) deposit in the North Daba Mountain, South Qinling, China: *Geological Journal*, v. 55, p. 4845–4863.
- Nie, X., Wang, Z., Chen, L., Yin, J., Xu, H., Fan, L., Wang, G., and An, B., 2020b, Trachytic magmatism and Nb-rare earth element mineralization in the Pingli area, North Daba Mountain: Insights from geochronology and geochemistry: *Geological Journal*, v. 55, p. 8225–8243.
- Nie, X., Wang, Z., Chen, L., Yin, J., and Wang, G., 2021, Monazites reveal timing and genesis of Nb-REE mineralization in trachyte from the Pingli area, North Daba Mountain, China: *Geosciences Journal*, v. 25, p. 605–617.
- Pavlidis, L., 1962, Geology and manganese deposits of the Maple and Hovey Mountains area, Aroostook County, Maine: U.S. Geological Survey Professional Paper 362, 116 p.

- Pollock, S.G., 2020, Bedrock geology of the Mooseleuk Mountain quadrangle, Maine: Maine Geological Survey, Open-File Map 20–1, scale 1:24,000.
- Ramsden, A., French, D., and Chalmers, D., 1993, Volcanic-hosted rare-metals deposit at Brockman, Western Australia: *Mineralium Deposita*, v. 28, p. 1–12.
- Rubin, J.N., Henry, C.D., and Price, J.G., 1989, Hydrothermal zircons and zircon overgrowths, Sierra Blanca Peaks, Texas: *American Mineralogist*, v. 74, p. 865–869.
- Sanford, R.F., Pierson, C.T., and Crovelli, R.A., 1993, An objective replacement method for censored geochemical data: *Mathematical Geology*, v. 25, p. 59–80.
- Shah, A.K., 2022, Airborne magnetic and radiometric survey, Munsungun region in northern Maine, 2021: U.S. Geological Survey data release, <https://doi.org/10.5066/P97VUIJS>.
- Shah, A.K., and Wang, C., 2022, Ground-based gamma spectrometry data collected in northern Maine (Version 2.0, September 2022): U.S. Geological Survey data release, <https://doi.org/10.5066/P9WFQ300>.
- Slack, J.F., Foose, M.P., Flohr, M.J.K., Scully, M.V., and Belkin, H.E., 2003, Exhalative and seafloor replacement processes in the formation of the Bald Mountain massive sulfide deposit, northern Maine: *Economic Geology Monograph* 11, p. 513–548.
- Slack, J.F., Beck, F.M., Bradley, D.C., Felch, M.M., Marvinney, R.G., and Whittaker, A.T.H., 2022, Potential for critical mineral deposits in Maine, USA: *Atlantic Geoscience*, v. 58, p. 155–191.
- Spandler, C., and Morris, C., 2016, Geology and genesis of the Toongi rare metal (Zr, Hf, Nb, Ta, Y and REE) deposit, NSW, Australia, and implications for rare metal mineralization in peralkaline igneous rocks: *Contributions to Mineralogy and Petrology*, v. 171, doi:10.1007/s00410-016-1316-y.
- Storey, M., 1982, Trachytic pyroclastics from Agua de Pau Volcano, Sao Miguel, Azores: Evolution of a magma body over 4,000 years: *Contributions to Mineralogy and Petrology*, v. 78, p. 423–432.
- Sun, S.-s., and McDonough, W.F., 1989, Chemical and isotopic systematics of oceanic basalts: Implications for mantle composition and processes, in Saunders, A.D., and Norry, M.J., eds., *Magma-tism in the ocean basins*: London, U.K., The Geological Society of London, p. 313–345.
- Taylor, W.R., Page, R.W., Esslemont, G., Rock, N.M.S., and Chalmers, D.I., 1995a, Geology of the volcanic-hosted Brockman rare-metals deposit, Halls Creek mobile zone, northwest Australia. I. Volcanic environment, geochronology and petrography of the Brockman volcanics: *Mineralogy and Petrology*, v. 52, p. 209–230.
- Taylor, W.R., Esslemont, G., and Sun, S.S., 1995b, Geology of the volcanic-hosted Brockman rare-metals deposit, Halls Creek mobile zone, northwest Australia. II. Geochemistry and petrogenesis of the Brockman volcanics: *Mineralogy and Petrology*, v. 52, p. 231–255.
- Tetra Tech, 2013, Preliminary economic assessment, Bokan Mountain rare earth element project: <https://ucore.com/docs/PEA.pdf>.
- U.S. Geological Survey, 2022a, List of critical minerals: <https://www.usgs.gov/news/national-news-release/us-geological-survey-releases-2022-list-critical-minerals>.
- 2022b, Mineral commodity summaries 2022: U.S. Geological Survey, 202 p., <https://doi.org/10.3133/mcs2022>.
- 2022c, Earth Mapping Resources Initiative (Earth MRI). Available at: <https://www.usgs.gov/special-topics/earth-mri?msckid=593a4d44cd3911ec8a6f73c37761643d>.
- Van Gosen, B.S., Verplanck, P.L., Seal, II, R.R., Long, K.R., and Gambogi, J., 2017, Rare-earth elements, in Schulz, K.J., DeYoung, Jr., J.H., Seal, II, R.R., and Bradley, D.C., eds., *Critical mineral resources of the United States—economic and environmental geology and prospects for future supply*: U.S. Geological Survey Professional Paper 1802, p. O1–O31, <https://doi.org/10.3133/pp18020>.
- Van Gosen, B.S., Verplanck, P.L., and Emsbo, P., 2019, Rare earth element mineral deposits in the United States: U.S. Geological Survey Circular 1454, 16 p.
- Verplanck, P.L., Mariano, A.N., and Mariano, Jr., A.N., 2016, Rare earth element ore geology of carbonatites: *Reviews in Economic Geology*, v. 18, p. 5–32.
- Wang, C., 2018, Bedrock geology of the Round Mountain quadrangle, Maine: Maine Geological Survey, Open-File Map 18–8, scale 1:24,000.
- 2019, Bedrock geology of the Jack Mountain quadrangle, Maine: Maine Geological Survey, Open-File Map 19–6, scale 1:24,000.
- 2021a, Bedrock geology of the Big Machias Lake quadrangle, Maine: Maine Geological Survey, Open-File Map 21–12, scale 1:24,000.
- 2021b, Bedrock geology of the Greenlaw Pond quadrangle, Maine: Maine Geological Survey, Open-File Map 21–2, scale 1:24,000.
- 2022a, Bedrock geology of the Carr Pond quadrangle, Maine: Maine Geological Survey, Open-File Map 22–6, scale 1:24,000.
- 2022b, Bedrock geology of the Fish River Lake quadrangle, Maine: Maine Geological Survey, Open-File Map 22–5, scale 1:24,000.
- Wang, K., Wang, L.-X., Ma, C.-Q., Zhu, Y.-X., She, Z.-B., Deng, X., and Chen, Q., 2021, Mineralogy and geochemistry of the Zhuxi Nb-rich trachytic rocks, South Qinling (China): Insights into the niobium mineralization during magmatic-hydrothermal processes: *Ore Geology Reviews*, v. 138, <https://doi.org/10.1016/j.oregeorev.2021.104346>.
- White, J.C., Parker, D.F., and Ren, M., 2009, The origin of trachyte and pantellerite from Pantelleria, Italy: Insights from major element, trace element, and thermodynamic modelling: *Journal of Volcanology and Geothermal Research*, v. 179, p. 33–55.
- Widom, E., Schmincke, H.-U., and Gill, J.B., 1992, Processes and timescales in the evolution of a chemically zoned trachyte: Fogo A, Sao Miguel, Azores: *Contributions to Mineralogy and Petrology*, v. 111, p. 311–328.
- Winchester, J.A., and van Staal, C.R., 1994, The chemistry and tectonic setting of Ordovician volcanic rocks in northern Maine and their relationship to contemporary volcanic rocks in northern New Brunswick: *American Journal of Science*, v. 294, p. 641–662.
- Winchester, J.A., van Staal, C.R., and Langton, J.P., 1992, The Ordovician volcanics of the Elmtree-Belledune inlier and their relationship to volcanics of the northern Miramichi Highlands, New Brunswick: *Canadian Journal of Earth Sciences*, v. 29, p. 1430–1447.
- Wyers, G.P., and Barton, M., 1987, Geochemistry of a transitional ne-trachyte-basalt-Q-trachyte lava series from Patmos (Dodecanesos), Greece: Further evidence for fractionation, mixing and assimilation: *Contributions to Mineralogy and Petrology*, v. 97, p. 279–291.
- Xiong, Y., Zhong, S., Li, Z., Huang, J., Lu, X., Du, Y., Wu, E., Li, Z., Zhao, S., and Zhu, Z., 2018, Geological characteristics and prospecting potential of niobium-tantalum deposit in the Tudiling area, Zhushan: *Resources Environment and Engineering*, v. 32, p. 1–7 (in Chinese with English abstract).
- Yan, S., Shan, Q., Niu, H.-C., Yu, X., Zhao, X., Zhao, X.-C., Zhang, H.-J., and Xiong, Y., 2021, Timing and genesis of the Tudiling trachyte Nb-Ta-Zr-REE deposit in the South Qinling (Central China): Implications for rare metal enrichment in extrusive peralkaline magmatic system: *Ore Geology Reviews*, v. 139, <https://doi.org/10.1016/j.oregeorev.2021.104535>.
- Yan, S., Niu, H.-C., Zhao, X., Zhang, Q.-B., Zhang, H.-J., and Zhao, X.-C., 2022, Rare metal enrichment of the Tianbao trachytic complex, North Daba Mountains (south Qinling): Insights from textures and geochemistry of trachytes and Nb-REE minerals: *Ore Geology Reviews*, v. 146, <https://doi.org/10.1016/j.oregeorev.2022.104948>.
- Yang, X.-Y., Sun, W.-D., Zhang, Y.-X., and Zheng, Y.-F., 2009, Geochemical constraints on the genesis of the Bayan Obo Fe-Nb-REE deposit in Inner Mongolia, China: *Geochimica et Cosmochimica Acta*, v. 73, p. 1417–1435.
- Yin, J.N., and Song, X., 2022, A review of major rare earth element and yttrium deposits in China: *Australian Journal of Earth Sciences*, v. 69, p. 1–25.

Chunzeng Wang is a geology professor at University of Maine at Presque Isle and on the graduate faculty of University of Maine and of Guilin University of Technology in China. He graduated with a B.A. in exploration geology from Guilin College of Geology in 1984, received an M.S. degree in structural geology from China University of Geoscience in 1989, and a Ph.D. in earth and environmental sciences from the City University of New York in 2001. Wang's research interests include tectonic and deformational history and mineral potential and metallogenesis of the northern Maine Appalachians, as well as in South China.

